Optik - International Journal for Light and Electron Optics 255 (2022) 168700

Contents lists available at ScienceDirect

Optik

journal homepage: www.elsevier.com/locate/ijleo

Development of neodymium (III) ions doped sodium fluoro-borate glass composite materials and study of the laser emission

Sk. Nayab Rasool [a,*], Sk. Shabeena [b], C.R. Kesavulu [c], E. Chandra Sekhar [d], S. Babu [e]

[a] Department of Physics, Rajeev Gandhi Memorial College of Engineering & Technology, Nandyal 518501, India
[b] Department of EEE, Rajeev Gandhi Memorial College of Engineering & Technology, Nandyal 518501, India
[c] SiC Laboratory, Centre for Materials for Electronics Technology (C-MET), Cherlapally, Hyderabad 500051, India
[d] Department of Chemistry, Rajeev Gandhi Memorial College of Engineering & Technology, Nandyal 518501, India
[e] Ceramics and Glass Institute (CSIC), C/Kelsen 5, Campus de Cantoblanco, 28049 Madrid, Spain

ARTICLE INFO

Keywords:
Fluoroborate glasses
Luminescence
Quantum efficiency
Stimulated emission cross-section
Melt quenching technique and Neodymium ions

ABSTRACT

Neodymium (III) ions doped sodium fluoro-borate (BCNF) glass materials have been prepared by the melt quenching method and Fourier transform infrared (FTIR) method was intended for the identification of the functional groups present in the BCNF host glass. X-ray diffraction (XRD) analysis is used for the study of structural details of the prepared glass composite materials. In order to study the spectroscopic properties of fabricated glasses, absorption, emission and decay measurements has been performed. Additionally, the spectroscopic properties of Nd^{3+} ions were analyzed using Judd-Ofelt theory. UV–Vis and Near-IR absorption spectra of glass composite samples reveal eleven significant peaks. Under the excitation of 808 nm laser diode, three near-IR emission bands are at around 876 nm, 1058 nm and 1331 nm from $^4F_{3/2} \rightarrow {}^4I_{9/2}$, $^4I_{11/2}$ and $^4I_{13/2}$ radiative transitions, respectively, were observed in the Nd^{3+} ions doped glass composite material. The lifetimes of this transition has been experimentally determined through decay profile studies. For all Nd^{3+} ion concentrations, the decay time curves of the $^4F_{3/2}$ level were essentially single exponential.

1. Introduction

Solid metal ions (SM^{+3}) doped glass composite materials are scientifically and technically significant materials due to their unique properties and prospects of use for incorporated optical lasers, amplifiers, Infrared-sensor and other flat panel technologies like plasma display panels [1]. Incorporation of the SM^{+3} into the various types of glass materials possess high luminescence efficiencies due to the excitations of the electrons present in the compositions [2–4]. The 4 f^n electronic level structures of these particles give some seemingly perpetual transitional intensities, which might be inhabited employing IR radiation. This type of transitional intensities, alongside with some meta-stable higher-lying levels, bring about strong visible emissions [3].

Glass materials have a long-range disordered and short-range ordered structure that can dissolve solid metal ions (Sm^{3+}, Nd^{3+}, Er^{3+}, etc.) quickly, allowing the properties of metal ions to be altered over a large range. As a result, the laser glass doped with solid metal ions such as rare earth (RE) ions is simple to make and has a number of desirable features, including a higher emission cross-section and greater quantum efficiencies [4]. As a result, RE elements have become one of the essential components for increasing

* Corresponding author.
E-mail address: rasoolphysics08@gmail.com (Sk. Nayab Rasool).

https://doi.org/10.1016/j.ijleo.2022.168700
Received 4 December 2021; Received in revised form 31 January 2022; Accepted 4 February 2022
Available online 7 February 2022

optical glass characteristics and developing prospective optical functions [3,4].

Among various host glass materials, the borate glass structure has some of the unique properties that includes high optical transparency, low melting point, high chemical stability, reasonableness and better RE ions solubility [5–7]. Based on the multiple properties of the borate glass materials, the host glass materials with boric acid can form the network and act as best host matrices for doping RE ions into the network structure for better applications. These doped glass materials are versatile materials to accept different types of cations and/or anions and also acts as an ion exchanger [8]. The previously mentioned properties of the doped glass materials supportive opportunities for speedy particle directing material and other huge applications like hosts for the laser, glass to metal seals and bio-similarity materials.

Presently, the solid-state lasers, where working at 1.06 μm wavelength has drawn in various consideration because of their potential applications, for example, photonic gadgets for high density optical storage, opto-electronics and medical diagnostics as well as optical communication system [6–8]. Concerning the luminescent properties, RE^{3+} ions like Nd^{3+} ions have become one of the popular active ions is due to its abundant lasing emissions in visible and IR regions [9]. The lasing action of Nd^{3+}-doped glass, for example, produces three major emission bands at roughly 876, 1058, and 1331 nm, which are attributed to the radiative transitions of $^4F_{3/2} \rightarrow {}^4I_{9/2}$, $^4F_{3/2} \rightarrow {}^4I_{11/2}$, and $^4F_{3/2} \rightarrow {}^4I_{13/2}$ respectively, in the near-infrared range [9,10]. Widely explored high power laser applications are obtained at 1.06 μm bands for the above mentioned three transitions [11], furthermore, the wide outflow at around 1.33 μm band is promising for O-band optical signal amplification [12] while laser emission in the 0.9 μm band allows for the fabrication of a device that emits blue radiation due to monolithic integration of laser emission [13]. Over the past decades, different examinations have been going with on the spectroscopic properties of neodymium (III) ions in various types of glass matrices including phosphate, borate, tellurite, and fluoride glass materials [14–26].

In the present study, we report on the optical properties of the Nd^{3+} doped fluoroborate (BCNFNd) glass materials to understand the improved near-IR band lasing emission yield. Although, studied about the optical properties, theoretical model Judd-Ofelt [27,28] estimations are completed from the oscillator strengths of the retention bands of 1.0 mol% Nd^{3+}doped BCNFNd10 glass materials to compute the laser distinctive properties of the $^4F_{3/2}$ excited level. Fluorescence measurements have been executed to recognize the radiative and non-radiative behavior of the BCNFNd glass materials.

2. Experimental

Table 1 represents the different chemical compositions used for the preparation of the Nd^{3+} ions doped BCNF glass compositions for the present study (Fig. 1 show the sample pictures of present studied glasses). The conventional melt-quenching technique is employed to formulate transparent glass materials using the analytical reagent grade of H_3BO_3, $CaCO_3$, NaF and Nd_2O_3 which were obtained from the sd-fine chemicals Mumbai India, as raw materials. According to the Table 1, the stoichiometric arrangements of these unrefined substances were mixed totally in an agate mortar and melted in an electric furnace at 1100 ℃ for 60 min using a porcelain crucible. Then the above compositions were poured onto the brass plate to obtain the various Nd^{3+} ions doped glass materials. The obtained glass materials were sufficiently strengthened at 350 ℃ temperature for 8 h in furnace and allowed to cool gradually to deliver the thermal stress allied by compositions of the doped glass materials during the extinguishing course. The refractive index "n" of the compositions (n = 1.650 for BCNFNd10 glass) was determined with an Abbe refractometer by mono bromo naphthalene as the interaction medium. The density "d" of Nd^{3+}ions doped glass material compositions (d = 2.365 gm/cc for BCNFNd10 glass) were measured by employing Archimedes principle. The XRD spectral data of the BCNF host glass was recorded utilizing JEOL 8530 X-beam diffractometer utilizing Cuka radiation. FTIR spectrum were recorded in the range 600–4000 cm^{-1} using Perkin-Elmer Paragon 500 FTIR spectrometer. Optical absorption study of the composed Nd^{3+} ions doped glass materials were recorded by utilizing Perkin–Elmer Lambda 350 UV–Vis spectrometer in the range of 400–1200 nm with a spectral resolution of ± 0.1 nm. The photo-luminescence and lifetime of $^4F_{3/2}$ level were estimated with the assistance of the third symphonious age (355 nm) of the Nd:YAG laser (Spectron Laser Sys. SL802G) as an excitation source.

3. Results and discussion

3.1. XRD pattern

The X-ray diffraction configuration were recorded in the range of $10^\circ \leq \theta \leq 80^\circ$ for the BCNF host glass shown in Fig. 2. It shows a wide dissipating at lower angles, demonstrating the long range structural disorder which affirm the amorphous nature of the glass

Table 1
Different chemical composition of neodymium (III) ions doped BCNF glass composite materials.

Glass label	Nd_2O_3 (mol%)	Glass composition
BCNFNd00	0.0	60 B_2O_3 + 20 CaO + 20 NaF_2
BCNFNd01	0.1	59.9 B_2O_3 + 20 CaO + 20 NaF_2 + 0.1Nd_2O_3
BCNFNd03	0.3	59.7 B_2O_3 + 20 CaO_3 + 20NaF_2 + 0.3Nd_2O_3
BCNFNd05	0.5	59.5 B_2O_3 + 20 CaO+ 20NaF_2 + 0.5Nd_2O_3
BCNFNd10	1.0	59.0 B_2O_3 + 20 CaO_3 + 20 NaF_2 + 1.0 Nd_2O_3
BCNFNd15	1.5	58.5 B_2O_3 + 20 CaO + 20 NaF_2 + 1.5Nd_2O_3
BCNFNd20	2.0	58.0 B_2O_3 + 20 CaO + 20 NaF_2 + 2.0 Nd_2O_3

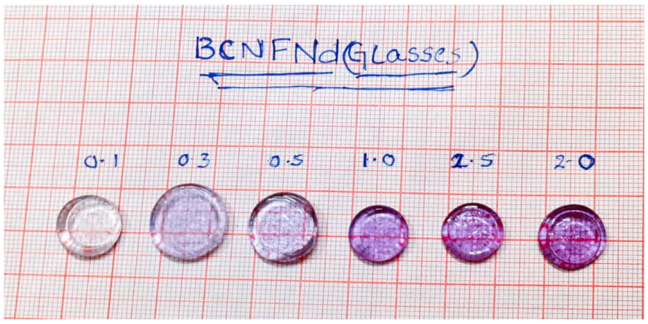

Fig. 1. Sample pictures of different concentration of neodymium (III) ions -doped BCNFNd glasses.

materials.

3.2. FTIR measurements

The FTIR spectrum of the BCNF host glass material was acquired in the range of 600–4000 cm^{-1} and used for the identification of functional groups in the host BCNF glass material. The results of the spectral data was shown in the Fig. 3 and the description of the spectral data was presented in Table 2, the band locations are assigned to multiple vibrational modes for all the compositions [29–34].

3.3. Optical band gap energy

Mott and Davids developed the following relationship for amorphous materials based on the absorption region [35,36],

$$\alpha h\upsilon = A^2(h\upsilon - E_g)^s - - - - - - - - - - - \quad (1)$$

Where Eg is the optical band gap and 's' takes different values of 2, 3, 1/2, and 1/3 corresponding to indirect allowed, indirect prohibited, direct allowed, and direct forbidden transitions, respectively. The band tailing parameter "A" is constant, and the energy of incident photons is hυ. The absorption coefficients α (υ) for BCNFNd10 glass sample were found near the absorption edge of photon energy. As a result, for indirect permitted transitions, the typical plot of $(\alpha h\upsilon)^{1/2}$ versus photon energy (hυ) (Tauc's plot) to find the value of optical band gap Eg is shown in Fig. 4, and the optical band gap value is given by 3.329 eV. It can be seen that $(\alpha h\upsilon)^{1/2}$ has a linear relationship with photon energy. This indicates that the transitions occurring in the current glass samples are of the indirect type at higher photon energy.

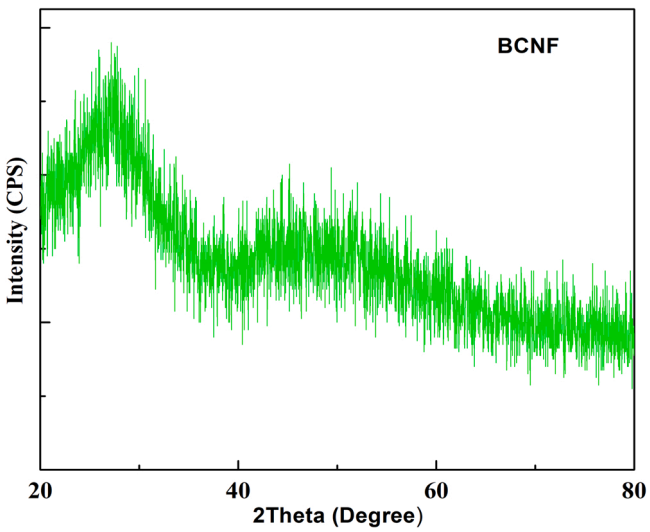

Fig. 2. XRD profile of BCNF host glass.

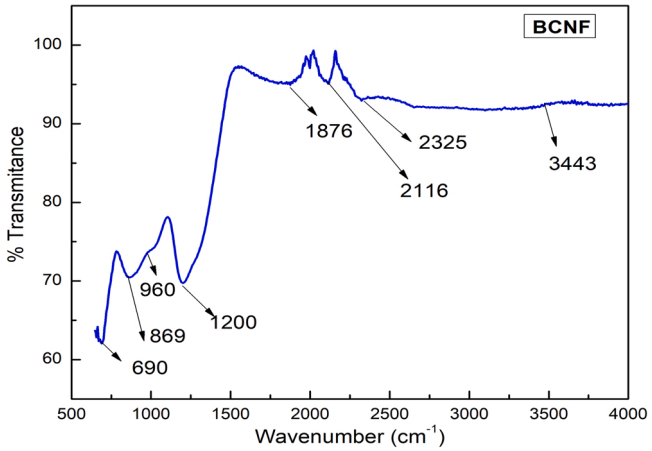

Fig. 3. FTIR spectrum of BCNF host glass material.

Table 2
FTIR analysis for the functional groups identification and their assignments for BCNF host glass material.

Wavenumber (cm^{-1})	FT-IR spectral assignment	Reference
690	B-O-B bending vibration modes	[29,30]
869,960	B-O-stretching vibrations of tetrahedral BO_4	[31–33]
1199	stretching B-O^- in BO_2O^- units	[31–33]
1296	B-O stretching in BO_2O^- triangle linked with BO_4 units	[31–33]
1600–2900	Hydrogen bonding in the glass matrix	[31–33]
3443	stretching vibrations of hydroxyl groups(O-H or H-O-H)	[34]

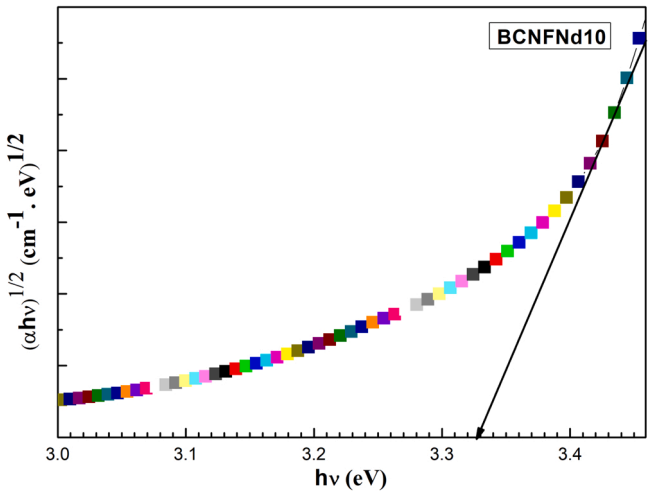

Fig. 4. Tauc's plot for indirect band gap of BCNFNd10 glass.

3.4. Results on refractive index, electronic polarizability and optical basicity

3.4.1. Refractive index

The refractive index (n) of an optical material is well known to play a significant role in the design of a new laser device. The value of 'n' can be determined using a variety of experimental methods. The value of 'n' was calculated experimentally using an Abbes refractometer and a sodium vapor lamp as a light source in this study, and it was found to be n = 1.650. The following formula [37] can be used to calculate the value of 'n' from the value of optical band gap energy (Eg).

$$\frac{n^2-1}{n^2+2} = 1 - \sqrt{\frac{E_g}{20}} \tag{2}$$

The refractive index of an optical substance can be calculated using the formula below, according to Duffy et, al. [38],

$$n = \quad -\ln[f_0](0.102\Delta\chi^*) \tag{3}$$

Where $\Delta\chi^*$ is called the optical electronegativity of the medium and it is given by

$$\Delta\chi^* = 0.2688E_g \tag{4}$$

The values of refractive index n (Eg) = 2.333 and n ($\Delta\chi^*$) = 2.393 obtained from Eq. (2) and from Eq. (3), respectively are very close and deviate slightly from those obtained from Abbes refractometer (n = 1.650). The deviation in the measurement of 'n' might be due to the experimental limits.

3.4.2. Oxide ion polarizability

The electronic polarizability is one of the important properties of materials and it is closely related to their applicability in the field of optics and electronics. The following empirical relation proposed by R.R. Reddy et al. [39] has been used to determine the oxide ion polarizability (α_0^{2-}) as

$$\alpha_0^{2-} \quad = \quad 4.624 - 0.7569\chi_{avg} \tag{5}$$

Where χ_{avg} represents the average electronegativity and it can be obtained using the following relation [40].

$$\chi_{ave} = \frac{\sum_{i=1}^{n} \chi i * Ni}{\sum_{i=1}^{n} Ni} \tag{6}$$

Where χ_i is called the Pauling electronegativity and N_i is the number of atoms of a particular species having electronegativity χi. The value of $\chi_{avg} = 2.761$ obtained for BCNFNd10 glass while the value of $\alpha_O{}^{2-} = 2.534 \times 10^{-24}$ cm^3.

3.4.3. Optical basicity

The theoretical basicity, Λth, in multi-component oxide glasses was computed using the equation presented by Duffy and Ingram [38] as given by

$$\Lambda th = X1\Lambda1 + X2\Lambda2 + X3\Lambda3 + \ldots \tag{7}$$

Where Λ1, Λ2 and Λ3 are basicities of the oxide components, and X1, X2 and X3 are their equivalent fractions (fraction of the total oxygen provided by the component oxide glass). The optical basicity for the glass systems in present study was calculated using relation,

$$\Lambda th = X_{B_2O_3}\Lambda(B_2O_3) + X_{CaCO_3} \quad \Lambda(CaCO_3) + X_{Nd_2O_3}\Lambda(Nd_2O_3) + \ldots \tag{8}$$

Where Λ (B_2O_3), Λ (CaO), Λ (NaF), Λ (Nd_2O_3) are the optical basicity values assigned to the constituent oxides and X $_{(B2O3)}$, X $_{(CaCO3)}$, X $_{(NaF)}$, X $_{(Nd2O3)}$ are the equivalent fractions of different oxides i.e. the contribution of oxide atom to the glass system. The optical basicity values of B_2O_3, CaO, NaF, Nd_2O_3 are 0.42, 1.00, 0.50 and 1.33, respectively, were taken from the literature [36,41,42]. The calculated

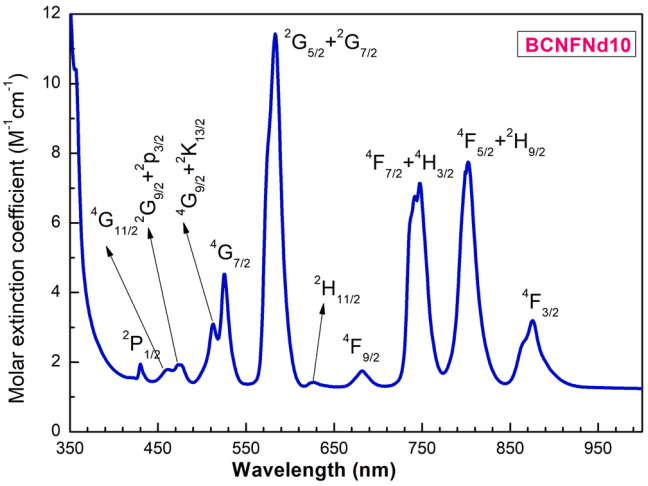

Fig. 5. Optical absorption spectrum of the selected neodymium (III) ions doped BCNFNd10 glass composite material.

Optical basicity of BCNFNd10 glass was 0.561. On the basis of refraction data, Duffy [38] proposed the following correlation

$$\Lambda th = 1.67 \quad \left[1 - \left(\frac{1}{\alpha_0{}^{2-}} \right) \right] \tag{9}$$

Where $\alpha_0{}^{2-}$ is the polarizability of oxide ions. According to Eq. (9), the basicity value is 0.786, it shows that the increase in polarizability results in an increase in optical basicity and consequently the refractive index.

3.5. Absorption spectrum and Judd-Ofelt Analysis

Fig. 5 displays the optical absorption spectra of BCNFNd10 glass materials in the range of 400–950 nm. The 4 f^3-4 f^3 electronic transitions are takes place in $^4I_{9/2}$ ground level of the neodymium (III) ions to various exciting levels and are responsible for the significant absorption bands. The values of the Nephelauxetic ratio (β) and bonding parameter (δ) can be used to determine the nature of the bonding between the neodymium (III) ions and their surroundings, It states that the ratio of the wavenumber of a certain neodymium (III) ions transition in the host matrix (υ_c) to the same aqua- ion transition (υ_a) [43]. Band position of the aqua- ion and transition assignments of the neodymium (III) ions were through based on the studies reported by Carnall et, al [43]. The Nephelauxetic ratio (β) and bonding parameter (δ) can be calculated using the relation [43].

$$\beta = \frac{\upsilon_c}{\upsilon_a} - - - - - - - - - - - \tag{10}$$

$$\delta = \frac{1 - \overline{\beta}}{\overline{\beta}} - - - - - - - - - - - \tag{11}$$

Here $\overline{\beta}$ referred as the average value of β.

Depending upon the sign of the δ, the neodymium (III) ions ligand may be covalent or ionic, the value of the δ of the BCNFNd10 glass were found to be − 0.3786, the ionic nature of the bonding between the neodymium (III) ions is shown by this number.

Table 3 shows the absorption bands' allocations, peak wavelength (λ), energy, and experimental (fexp) and calculated (fcal) oscillator strengths. Between the exploratory (fexp) and determined (fcal) oscillator strengths, three Judd-Ofelt intensity parameters, i. e., $\Omega_\lambda = 2$, 4 and 6 are determined through utilizing the least square fit methodology which are described somewhere else [19,23]. From the absorption spectrum, it is noticed that one particular transition namely $^4I_{9/2} \rightarrow {}^4G_{5/2}$ transition observed at 583 nm band is more intense than other transitions and having large oscillator strengths. This transition is known as the hypersensitive transition, since it adheres to the norms of selection rules of $\Delta L \leq 2$; $\Delta S = 0$ and $\Delta J \leq 2$, $|\Delta S| = 0$; $|\Delta L| \leq 2$ and $|\Delta J| \leq 2$ [21]. The oscillator strength of hypersensitive transitions is generally very large and it is extraordinarily impacted by the ion-ligand bonding environment.

As per recent literature survey [19,44], Ω_2 (8.99×10^{-20} cm^2) is associated to the covalence among neodymium (III) ions and ligand anions as well as the asymmetry of the local environment around the site of Nd^{3+} ions. In this regard, the lower the Ω_2 is more centro-symmetric the ion site and the more ionic the ligand compound connections. As such, the prepared Nd^{3+} ions doped glass composites have low covalence and highly ionic specificity between the doped neodymium (III) ions and ligand anions along together with low asymmetry of the surrounding atmosphere of neodymium (III) ions. Thus, Ω_2 won't influence the stimulated emission parameters at near-IR region [45]. Though, the Ω_4 (*12.01* $\times 10^{-20}$ cm^2) and Ω_6 (*12.68* $\times 10^{-20}$ cm^2) straightforwardly affect the assurance of spectroscopic properties. The spectroscopic quality factor χ ($\Omega_4/\Omega_6 = 0.96$) is a distinguished ratio that may be used to estimate relative weight factors for $^4F_{3/2} \rightarrow {}^4I_{9/2}$ and $^4F_{3/2} \rightarrow {}^4I_{11/2}$ fundamental intensities [19].

The trend in the Ω_λ parameters of $\Omega_2 < \Omega_4 < \Omega_6$, which is similar to that observed for BZBNd [17], LHG-80 [18] and TZNLN [19] glasses. It is found that the spectroscopic quality factor (χ) of the prepared composite glass materials can reach 0.96, and is better results than the zinc phosphate (0.75), BZBNd (0.83), LHG-80 (0.91), TZNLN (0.86), borate (0.65), fluorohosphate (0.37) and SBiLNd (0.88) of previous reports [16–22]. Furthermore, it tends to be anticipated that the intensity of $^4F_{3/2} \rightarrow {}^4I_{11/2}$ transition in the glass

Table 3
Assignment of absorption transitions, peak location (λ, nm), energy (cm^{-1}), experimental (f_{exp} x 10^{-6}) and calculated (f_{cal} x10^{-6}) oscillator strengths for BCNFNd10 glass.

Transition $^4I_{9/2}\rightarrow$	Wavelength λ (nm)	Energy (cm^{-1})	Oscillator strengths	
			f_{exp}	f_{cal}
$^4F_{3/2}$	875	11415	5.57	6.48
$^4F_{5/2} + {}^2H_{9/2}$	802	12468	17.20	15.97
$^4F_{7/2} + {}^4S_{3/2}$	747	13386	18.76	19.40
$^4F_{9/2}$	681	14662	1.35	1.50
$^2H_{11/2}$	626	15948	0.26	0.42
$^4G_{5/2}$	583	17152	47.67	47.68
$^4G_{7/2}$	525	19011	9.74	9.31
$^4G_{9/2} + {}^2K_{15/2}$	513	19531	0.42	1.4
$^4G_{11/2} + {}^2D_{3/2} + {}^2P_{3/2} + {}^2G_{9/2}$	461	21786	0.54	2.7
$^2P_{1/2}$	430	23256	0.98	1.66
	$\delta_{rms} = \pm 0.96$			

composites will be larger than that $^4F_{3/2} \rightarrow {}^4I_{9/2}$ transition in the formulated glass materials. It is normal that the samples have better spectroscopic quality around 1.06 μm. In this study, new approaches are described by the JO theory with a few radiative properties like transition probabilities (A_R), experimental lifetime (τ_R) of $^4F_{3/2}$ energy level, branching ratios (β_R), and peak stimulated emission cross-section (σ (λp)) [19,23].

3.6. Luminescence properties

Near-IR luminescence spectra of the different concentrations of neodymium (III) ions doped BCNFNd glass composites are shown in Fig. 6. In the present figure, the major emission peaks are at 876, 1058, and 1331 nm corresponding to the $^4F_{3/2} \rightarrow {}^4I_J$ ($J = 9/2$, 11/2, and 13/2) transitions. The excitation of electron transitions and emission transitions of the neodymium (III) ions doped BCNFNd10 glass composites are represented in the energy level diagram in Fig. 7. The radiative characteristics of the composed composite glass materials were assessed and including emission peak wavelengths (λp), effective line bandwidths ($\Delta\lambda_{eff}$), stimulated emission cross-section (σ (λp)), experimental (βexp), and computed branching ratios (β_R) were clearly recorded in Table 4. Due to its more prominent emission cross-section, the $^4F_{3/2} \rightarrow {}^4I_{11/2}$ transition has more potential for lasing action as shown in Table 4. The saturation intensity, $I_s = hc / \lambda\, \sigma(\lambda_p)\tau_{exp}$, which depends on the central glass material and the result of the emission cross-section of the lasing transition and the test lifetime of the excited level [46], is directly proportional to the pump input power required to reach the threshold for continuous wave (cw) laser operation. The I_s values for the $^4F_{3/2} \rightarrow {}^4I_{11/2}$ laser transition in different Nd^{3+}-doped glasses are compared in Table 5. The current glass's I_s value is greater than that of LHG-80, BZBNd10, bismuth-borate, PKACaFNd10 and silicate [17,19,22–25] glasses.

3.7. Decay measurements

Fig. 8 shows the investigational decay profiles of the $^4F_{3/2}$ excited level of the Nd^{3+} ions in BCNFNd glass composite material, monitored at $^4F_{3/2} \rightarrow {}^4I_{11/2}$ transition (emission at 1.06 μm). The initial e-folding times to the decay intensity were utilized to derive the experimental life times for the $^4F_{3/2}$ level. Because of the low action of ligands on doped Nd^{3+} ions, the decay time curves are essentially solitary exponential even an greater Nd^{3+} ions concentrations (up to 2.0 mol percent). For 0.1, 0.3, 0.5, 1.0, 1.5 and 2.0 mol % of Nd^{3+} ions, the lifetimes of the $^4F_{3/2}$ level in the prepared doped glass material are 89, 74, 68, 45, 33, and 20 μs, respectively. The reduction in lifetime might be owing to the Nd^{3+} ions concentration quenching action. The non-radiative decay (W_{NR}) cycles may clarify the disparity among the experimental ($\tau_{exp} = 45$ μs) and radiative life times ($\tau_R = 110$ μs) for the $^4F_{3/2}$ level of Nd^{3+} ions in BCNFNd10 glass materials.

The non-radiative decay rate (W_{NR}) for the $^4F_{3/2}$ level can be determined utilizing the following condition.

$$W_{NR} = 1/\tau_{exp} - 1/\tau_{rad}.$$

Where τ_{exp} and τ_{rad} are the experimental and radiative lifetimes, respectively.

In general, there are four non-radiative decay mechanisms that contribute to the decline of the emission level's exp,

$$W_{NR} = W_{MP} + W_{CQ} + W_{ET} + W_{OH}$$

The non-radiative decay rates compared to multiphononrelaxation, concentration quenching, energy move to another doping contamination, and hydroxyl (OH^-) functional groups, are W_{MP}, W_{CQ}, W_{ET}, and W_{OH}, accordingly.

A fluoro-borate glass's typical phonon energy is roughly 1300 cm^{-1} [47]. There is a 5400 cm^{-1} energy gap between the metastable $^4F_{3/2}$ level and its lower $^4I_{15/2}$ level. Hence four phonons are needed to bridge the gap. Therefore, multi phonons relaxation plays a significant role in the non-radiative decay process in the present Nd^{3+} doped systems. Non-radiative decay by concentration quenching (W_{CQ}) arises with increase in active ion concentration. This term also important in the present glass system as is evident from the decrease lifetimes of $^4F_{3/2}$ level in BCNFNd (from 89 to 20 μs) glasses when the concentration of Nd^{3+} ions is increased from 0.1 to 2.0 mol%. The exponential nature of the decay curves indicates the absence of energy transfer process in the current BCNFNd glass systems.

The luminescence quantum efficiency (η) of an emission level $^4F_{3/2}$ can be calculated by using the equation.

$$\eta\ \% = \tau_{exp} / \tau_r.$$

Table 5 presents comparison of laser quality factors of 1.06 μm level of neodymium (III) ions in BCNFNd10 with other various reported neodymium (III) ions doped systems [17,19,22–25]. From Table 5 the present BCNFNd10 glass's optical gain parameter is 83.60×10^{-25} cm^2 which is greater than that of BZBNd10 (64.23×10^{-25} cm^2), TZNLN (65.76×10^{-25} cm^2), SBiLNd (67.05×10^{-25} cm^2) and lower than that of PKACaFNd10 (111.32×10^{-25} cm^2) and BNf5Nd10 (185.24×10^{-25} cm^2) [17,19,22,23,25] glasses.

4. Conclusions

In summary, the optical properties of different Nd^{3+} -doped BCNF glasses have been investigated. The optical spectral data were used to evaluate the value of indirect bandgap. The laser quality factors such as effective emission bandwidths, figure of merit, gain bandwidths, optical gain parameters and saturation intensity for $^4F_{9/2} \rightarrow {}^4I_{11/2}$ transition have been calculated and compared with other reported glasses. The stimulated emission cross section for BCNFNd10 glass is found to be higher than those of LHG-80,

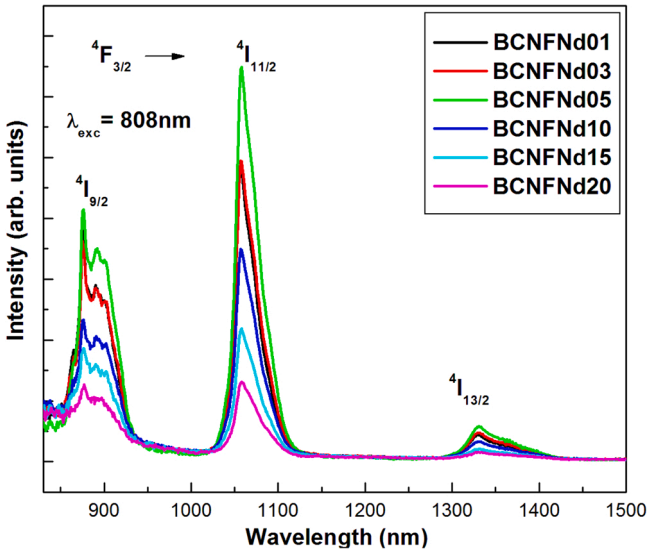

Fig. 6. Near-IR photoluminescence spectra of neodymium (III) ions present in the BCNFNd glass materials for different concentration of Nd_2O_3.

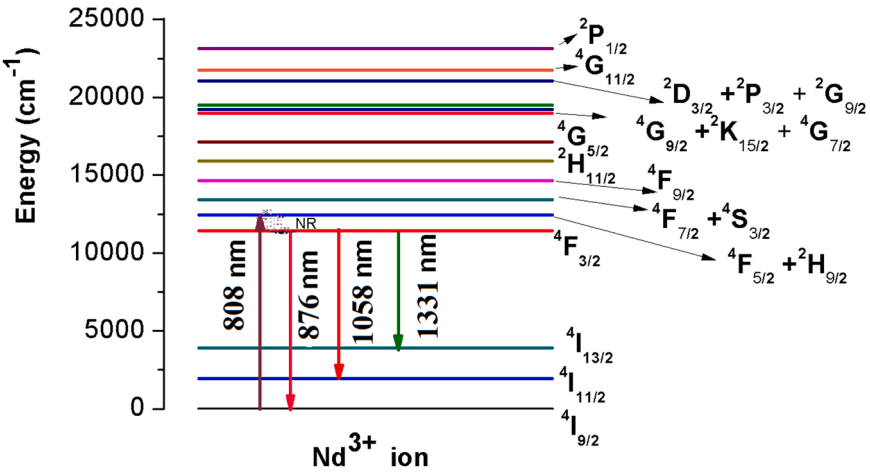

Fig. 7. Energy level diagram of 1 mol% of neodymium (III) ions in doped BCNF glass.

Table 4
Emission peak positions (λ_p, nm), Electric dipole line strength (S_{ed}, x 10^{+22}) experimental (β_{exp}) and calculated (β_{cal}) branching ratios, transition probabilities (A_R,s^{-1}), effective band widths ($\Delta\lambda_{eff}$, nm) and stimulated emission cross-section ($\sigma(\lambda_p)$ x 10^{-20} cm^2) for neodymium (III) ions in BCNFNd10 glass.

Transition $^4F_{3/2}$	λ_p (nm)	Electric dipole line strength (S_{ed})	Branching ratios		A_R	$\Delta\lambda_{eff}$	σ (λ_p)
			β_{exp}	β_{cal}			
$^4I_{9/2}$	876	346.32	0.42	0.32	3800	23.48	4.64
$^4I_{11/2}$	1058	685.59	0.48	0.59	4410	35.43	7.60
$^4I_{13/2}$	1331	268.06	0.1	0.09	858	63.04	2.08
		τ_r = 110 μs					

BZBNd10, bismuth-borate, PKACaFNd10 and silicate glasses. Hence, the presented BCNFNd glass materials can also be considered as suitable and very promising candidate for developing high energy high power 1.06 μm solid state laser.

Declaration of Competing Interest

The authors declare that they have no known competing financial interests or personal relationships that could have appeared to

Table 5
Comparison of laser quality factors of 1.06 μm level of neodymium (III) ions in BCNFNd10 with other various reported neodymium (III) ions doped systems.

Glass	λ_p (nm)	$\Delta\lambda_{eff}$ (nm)	$\sigma(\lambda_p)$ (x 10^{20} cm^2),	$\sigma(\lambda_p)$ x $\Delta\lambda_{eff}$ (x 10^{-26} cm^3)	τ_r (μs)	τ_{exp} (μs)	$\sigma(\lambda_p)$ x τ_r (x 10^{-25} cm^2)	$\sigma(\lambda_p)$ x τ_{exp} (x 10^{-25} cm^2)	η (100%)	I_s (x 10^8 W/m^2)	W_{NR} (s^{-1})	References
BCNFNd10	1058	35.43	7.60	26.9	110	45	83.60	34.2	41	5.48	13100	[P.W]
BZBNd10	1063	29.00	4.43	1.25	145	62	64.23	27.4	43	2.78	9100	[17]
TZNLN	1061	28.35	4.27	12.1	154	136	65.76	58.07	88	3.22	900	[19]
SBiLNd	1058	34.00	2.33	7.9	290	263	67.05	61.27	91	3.06	300	[22]
PKACaFNd10	1057	30.00	5.06	15.2	220	154	111.32	77.92	70	2.41	1900	[23]
BiZNd	–	–	–	–	169	83	–	–	49	6.66	6100	[24]
BNaNf	–	–	–	–	347	151	–	–	43	2.96	3700	[25]
BNf5Nd10	1062	19.00	4.40	8.3	421	153	185.24	67.3	36	2.78	4200	[25]
Bismath-borate	–	–	–	–	175	71	–	–	41	2.82	8400	[26]

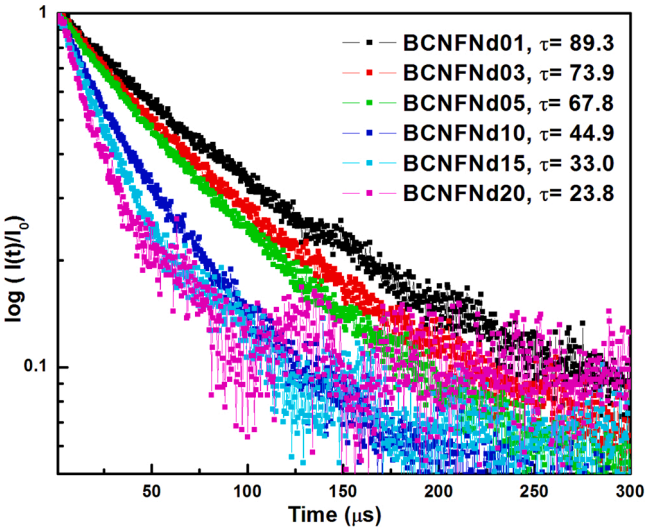

Fig. 8. The life time-decay profiles of the $^4F_{3/2}$ level of different concentrations of neodymium (III) ions in BCNFNd glasses.

influence the work reported in this paper.

References

[1] Y.A. Lakshmi, K. Swapna, K.S.R.K. Reddy, M. Venkateswarlu, Sk Mahamuda, A.S. Rao, J. Lumin 211 (2019) 39.
[2] J. Rajagukguk, R. Situmorang, Fitrilawati, M. Djamal, R. Rajaramakrishna, J. Kaewkhao, P.H. Minh, J. Lumin 216 (2019), 116738.
[3] Elena A. Anashkina, Fibers 8 (2020) 30.
[4] M. Xianfeng, Z. Qitu, L. Chunhua, et al., J. Rare Earths 22 (2004) 81.
[5] D. Rajesh, A. Balakrishna, Y.C. Ratnakaram, Opt. Mater. 35 (2012) 108.
[6] S. Berneschi, G.C. Righini, S. Pelli, Appl. Sci. 11 (2021) 4610.
[7] A. Renuka Devi, C.K. Jayasankar, Mat. Chem. Phys. 42 (1995) 106.
[8] A. Sarakovskisa, G. Krieke, J. Eur. Ceram. Soc. 35 (2015) 3665.
[9] M. Shoaib, G. Rooh, N. Chanthima, H.J. Kim, J. Kaewkhao, Optik 199 (2019), 163218.
[10] T. Wei, Y. Tian, C. Tian, et al., J. Alloy. Compd. 618 (2015) 95.
[11] C.R. Kesavulu, H.J. Kim, S.W. Lee, J. Kaewkhao, N. Wantana, E. Kaewnuam, S. Kothan, S. Kaewjaeng, J. Alloy. Compd. 695 (2017) 590.
[12] H.K. Dan, D.C. Zhou, Z.W. Yang, Z.G. Song, X. Yu, J.B. Qiu, J. Non-Cryst. Solids 414 (2015) 21.
[13] T.F. Xue, L.Y. Zhang, J.J. Hu, M.S. Liao, L.L. Hu, Opt. Mater. 47 (2015) 24.
[14] J.A. Jiménez, M. Sendova, J. Chem. Phys. 162 (2015) 425.
[15] X. Long, J. Bai, X. Liu, W. Zhao, G. Cheng, Chin. Opt. Lett. 11 (2013), 102301.
[16] K. Upendra Kumar, P. Babu, Kyoung Hyuk Jang, Hyo Jin Seo, C.K. Jayasankar, A.S. Joshi, J. Alloy. Compd. 458 (2008) 509.
[17] B. Shanmugavelu, V. Venkatramu, V.V. Ravi Kanth Kumar, Spectrochim. Acta Part A 122 (2014) 422.
[18] J.H. Campbell, T.I. Suratwala, J. Non-Cryst. Solids 263/264 (2000) 318.
[19] S. Surendra Babu, R. Rajeswari, K. Jang, C. Eun Jin, K. Hyuk Jang, H. Jin Seo, C.K. Jayasankar, J. Lumin 130 (2010) 1021.
[20] K. Vijaya Kumar, A. Suresh Kumar, Opt. Mater. 35 (2012) 12.
[21] Y. Tian, J. Zhang, X. Jing, S. Xu, Spectrochim. Acta Part A Mol. Bio. Spec. 98 (2012) 355.
[22] C. Tian, Xi Chen, Yu Shuibao, Solid State Sci. 48 (2015) 171.
[23] Rasool S.K. Nayab, T. Sasikala, A.M. Babu, L.R. Moorthy, C.K. Jayasankar, Spectrochim. Acta Part A Mol. Biomol. Spectrosc. 180 (2017) 193.
[24] G. Gupta, A.D. Sontakke, P. Karmakar, K. Biswas, S. Balaji, R. Saha, R. Sen, K. Annapurna, J. Lumin 149 (2014) 163.

[25] R.T. Karunakaran, K. Marimuthu, S. Arumugam, S. Surendra Babu, S.F. Leon-Luis, C.K. Jayasankar, Opt. Mater. 32 (2010) 1035.
[26] Y. Chen, Y. Huang, M. Huang, R. Chen, Z. Luo, J. Am. Ceram. Soc. 88 (2005) 19.
[27] B.R. Judd, Phys. Rev. 127 (1962) 750.
[28] G.S. Ofelt, J. Phys. Chem. 37 (1962) 511.
[29] F.L. Galeener, G. Lucovsky, J.C. Mikkelsen Jr., Phys. Rev. B 22 (1980) 3983.
[30] S. Liu, G. Zhao, X. Lin, H. Ying, J. Liu, J. Wang, G. Han, J. Solid State Chem. 181 (2008) 2725.
[31] G.E. Jellison, P.J. Bray, J. Non-Cryst. Solids 29 (1978) 187.
[32] R.T. Karunakaran, K. Marimuthu, S.S. Babu, S. Arumugam, Phys. B 404 (2009) 3995.
[33] J. Schwarz, H. Ticha, J. Optoelectron. Adv. Mater. 5 (2003) 69.
[34] W.A. Pisarski, J. Pisarska, M. Maczka, W. Ryba-Romanowski, J. Mol. Struct. 792–793 (2006) 207.
[35] M.A. Baki, F.A.A. Wahab, A. Radi, F.E. Diasty, J. Phys. Chem. Solids 68 (8) (2007) 1457.
[36] P. Chimalawong, J. Kaewkhao, C. Kedkaew, P. Limsuwan, J. Phys. Chem. Solids 71 (2010) 965.
[37] V. Dimitrov, S. Sakka, J. Appl. Phys. 79 (1996) 1736.
[38] J.A. Duffy, M.D. Ingram, D. Uhlman, N. Kreidl (Eds.), Am. Ceram. Soc., Westerville, 1991.
[39] R.R. Reddy, Y.N. Ahammed, P.A. Azeem, K.R. Gopal, T.V.R. Rao, J. Non-Cryst. Solids 286 (2001) 169.
[40] R. Asokamani, R. Manjula, Phys. Rev. B 39 (1989) 4217.
[41] Vesselin Dimitrov, Takayuki Komatsu, J. Solid. State Chem. 163 (2002) 100.
[42] Xinyu Zhaoa, Xiaoli Wangb, Hai Lina, Zhiqiang Wanga, Phys. B 392 (2007) 132.
[43] W.T. Carnall, P.R. Fields, K. Rajnak, J. Chem. Phys. 49 (1968) 4424.
[44] N.O. Dantas, E.O. Serqueira, A.C.A. Silva, A.A. Andrade, S.A. Lourenço, Braz. J. Phys. 43 (2013) 230.
[45] I. Pal, A. Agarwal, S. Sanghi, M.P. Aggarwal, S. Bhardwaj, J. Alloy. Compd. 587 (2014) 332.
[46] J. Azkargorta, I. Iparraguirre, R. Balda, J. Fernandez, E. Denoue, J.L. Adam, J. IEEE, Quant. Electron. 30 (1994) 1862.
[47] M. Djamal, L. Yuliantini, R. Hidayat, N. Rauf, M. Horprathum, R. Rajaramakrishna, K. Boonin, P. Yasaka, J. Kaewkhao, V. Venkataramu, S. Kothan, Opt. Mater. 107 (2020), 110018.